Accelerated ReaxFF Simulations of Vitrimers with Dynamic Covalent Adaptive Networks

Yiwen Zheng,[†] Vikas Varshney,[‡] and Aniruddh Vashisth[*,†]

[†]*Department of Mechanical Engineering, University of Washington, Seattle, WA, USA*

[‡]*Materials and Manufacturing Directorate, Air Force Research Laboratory, Wright-Patterson Air Force Base, Dayton, OH, USA*

E-mail: vashisth@uw.edu

Abstract

Vitrimers are a novel class of sustainable polymers with dynamics covalent adaptive networks driven by bond exchange reactions between different constituents, making vitrimers reprocessable and recyclable. Current modeling approaches of bond exchange reactions fall short in realistically capturing the complete reaction pathways, which limit our understanding the viscoelastic properties of vitrimers. This research addresses these limitations by extending and employing Accelerated Reactive Molecular Dynamics (ReaxFF) technique, thus enabling a more accurate representation of vitrimer viscoelastic behavior at the molecular level. Bayesian optimization is employed to select force field parameters within the Accelerated ReaxFF framework, and an empirical function is proposed to model temperature dependency, thereby controlling reaction probabilities under varying temperatures. The extended framework is employed to simulate non-isothermal creep behavior of vitrimers under different applied stress levels, heating rates and numbers of reactions. The simulation results agree with experimental findings in literature, validating the robustness of the framework.

Introduction

Thermosetting resins are widely recognized for their exceptional mechanical properties, strong adhesive qualities, and robust chemical resistance, making them indispensable in numerous industrial applications such as coatings, adhesives, composites, and electronic materials.[1,2] These thermosetting polymers form a highly cross-linked network upon curing, which imparts their desirable properties. However, this cross-linked structure also leads to an inability to be reprocessed or recycled, posing significant challenges for sustainability and end-of-life management.[3–5] The development of vitrimer polymers represents an exciting advancement in polymer science, addressing the limitations of traditional thermosetting resins like epoxy. Vitrimers are a class of polymers that combine the mechanical strength of thermosets with the reprocessability of thermoplastics.[6,7] They achieve this through the associative covalent adaptive network composed of dynamic covalent bonds that can exchange with each other without loss of network integrity.[8] This provides the macromolecular network adaptive nature and allows the network to rearrange under specific conditions while conserving its crosslink density. This unique characteristic enables vitrimers to be repaired,[9–11] reshaped,[12,13] and recycled,[14–16] thus offering significant advantages in terms of sustainability and lifecycle management.[17–20]

Apart from experimental methods, theoretical models and simulations are exciting tools to probe fundamental principles that dominate the behavior of these materials.[21] Researchers have used various methods to simulate vitrimers. Continuum and meso-scale models have been employed which include theoretical models,[22] patchy particle models,[23,24] and coarse-grain models.[25–28] While these models align well with specific experimental results, they lack the granularity to capture the heterogeneity and site-specific network evolution during the healing process. In addition, the commonly adopted approaches to speed up reaction kinetics use elevated temperatures that can lead to undesirable side reactions. On the other hand, methods such as ab initio simulations,[29,30] and hybrid molecular dynamics (MD) - Monte Carlo (MC) simulations have been applied to investigate vitrimer behavior as well.[31–33]

However, while the ab initio methods can simulate only a small number of atoms which prohibit the simulations of polymer networks, hybrid MD-MC approach is restricted to the coarse-grained scale and lacks sufficient atomistic details of reactive atoms.

One of the outstanding challenges for vitrimer polymers is understanding their creep performance under different conditions such as elevated temperatures and external stresses.[34–36] To this end, molecular dynamics simulations have shown to be useful for providing molecular insights into the structural, dynamical, and thermodynamical properties of polymer materials at the atomic level, enabling the prediction and analysis of material behavior under various conditions.[37,38] Atomistic simulations have been successful in providing insights about polymer structure-property relationships.[39–42] Previous works demonstrated that classical molecular dynamics can simulate vitrimer behavior using the "cut-off" method for bond exchange.[43–47] In this method, bonds are formed based purely on the proximity of reacting atoms. However, this approach has limitations as it evaluates the likelihood of reactions occurring based solely on the distance between reactive sites, without considering the actual reaction pathway. Additionally, the unbounded number of simultaneous reactions that may occur results in an indefinite reaction rate and limits the ability to capture the reaction rate's dependence on catalyst concentration, as observed in real experiments. Furthermore, this simulation setup involves frequent equilibration steps after formation of new bonds during the simulation, which disrupts simulation continuity and may introduce additional artifacts.

Reactive molecular dynamics or ReaxFF is able to bridge the gap between density functional theory (DFT) and MD simulations as it can simulate reactive dynamics in large systems while being computationally feasible.[48] Specially for polymers, ReaxFF has shown promise for simulating polymer crosslinking,[39] degradation,[49] thermo-mechanical characterization,[44] and adhesion.[50] Previous works have used the "cut-off" method to capture polymer reactions with slow kinetics, ignoring the reaction pathway and may lead to unrealistic "after-reaction" configurations that would not be feasible in real systems. Vashisth et al. have developed a new method within the framework of ReaxFF that can simulate slow reac-

tions in computationally feasible time; this method is called Accelerated ReaxFF.[51] In this method, the reactants are monitored until they achieve a configuration conducive to initiating a reactive event. Once this configuration is reached, the reactants are supplied with energy equivalent to or slightly exceeding the reaction energy barrier. This energy input is designed to help the reactants overcome the barrier for the bond exchange process and transition into the desired products. This approach allows for the simulation of bond exchange reactions (BERs) at realistic, lower temperatures, thus closely emulating actual chemical reactions while minimizing unintended high-temperature side reactions. This method has shown to capture the effect of molecular chemistry on crosslink density of thermosets and resulting thermo-mechanical properties of these polymers,[40,49,52] as well as reverse Diels–Alder reactions in polymer networks.[53]

In this paper, we use the Accelerated ReaxFF framework to investigate the non-isothermal creep behavior of vitrimers. A novel scheme based on Bayesian optimization is developed to select the appropriate force parameters for the restraint energy. An empirical equation is further introduced to define force parameters as a function of temperature and achieves temperature-dependent BER probabilities in ReaxFF simulations. This setup is used to simulate non-isothermal creep of vitrimers under varying external stimuli, i.e., applied stress, heating rate, and number of reactions (reflective of catalyst concentrations). Their effect on creep strain is captured, which is consistent with experimental findings in literature. During creep, the BERs start to develop between 300 and 500 K, agreeing well with the topology freezing transition temperature observed in experiments for transesterification vitrimers. In addition, we analyze the evolution of free volume and distribution of reactive atom towards providing valuable insights into creep mechanisms at the atomistic scale.

Methods

Accelerated ReaxFF simulations

ReaxFF is a molecular dynamics simulation method incorporating the bond order concept to account for dynamic interactions between atoms.[48,54] This technique ensures a seamless transition among non-bonded states and single, double, or triple bonded states, allowing for the exploration of chemical reactions involving bond formation and dissociation.[48] The total interaction energy in ReaxFF is composed of multiple contributions, which are represented as

$$E_{\text{system}} = E_{\text{bond}} + E_{\text{over}} + E_{\text{under}} + E_{\text{val}} + E_{\text{tors}} + E_{\text{vdW}} + E_{\text{Coulomb}} + E_{\text{lp}} + E_{\text{H-bond}} + E_{\text{rest}} \quad (1)$$

The total energy of the system (E_{system}) consists of bonded or covalent interactions (which are bond order dependent) and non-bonded interactions. Bond order dependent terms include bond energy (E_{bond}), over coordination (E_{over}), under coordination (E_{under}) and hydrogen bond interactions ($E_{\text{H-bond}}$). Energy penalty terms include torsion angle energy (E_{tors}), valence-angle energy (E_{val}), and lone pair energy (E_{lp}). Non-bonded interactions include van der Waals (E_{vdW}) and Coulombic interactions (E_{Coulomb}). Bond order is calculated based on interatomic distances and updated at each molecular dynamics or energy minimization step. Non-bonded interactions, such as van der Waals and Coulomb terms, are considered for all atom pairs. Atomic charges are derived and updated using the electronegativity equalization method.[55] The parameters for the force field, which describe energy terms, are typically optimized through quantum mechanical calculations and experimental data.

In the Accelerated ReaxFF framework, the algorithm monitors the distances between labeled reactive atoms at each time step. Once a group of atoms falls within the predefined distance ranges, an external restraint energy (E_{rest}), or "bond boost",[56] is added to pairs of reactive atoms for a designated number of steps N. This additional energy moves the atoms

either closer together or farther apart, facilitating bond formation or dissociation and thereby accelerating the chemical reactions between reactive species. The number of reactions taking place simultaneously is limited by a predefined number of boosts. For each atom pair, the restraint energy added at time step t is expressed as

$$E_{\text{rest}}^{t} = F_1 \left(1 - e^{-F_2\left(R_{ij}^{t} - R_{12}^{t}\right)^2}\right) \tag{2}$$

where F_1 and F_2 are force parameters, R_{12}^{t} is the desired distance and R_{ij}^{t} is the distance between atoms i and j at time step t. The target distance R_{12}^{t}, calculated by the Accelerated ReaxFF program and changing at each time step, depends on the initial distance R_{ij}^{0} and a predefined final desirable distance R_{12} after N steps, i.e.,

$$R_{12}^{t} = R_{ij}^{0}\left(1 - \frac{t}{N}\right) + R_{12}\frac{t}{N}. \tag{3}$$

When R_{ij}^{t} significantly deviates from R_{12}^{t}, the resistance of the system to the restraint is increased, leading to a higher E_{rest}. This energy is applied to reactive sites to accelerate bond formation or dissociation, guiding the atoms toward the desired distance R_{12} within N steps. For bond formation, R_{12} is set to the equilibrium bond length, while for bond dissociation, it is set to 2.5 Å to ensure sufficient separation. Notably, all restraints are one-sided, acting only to move the atoms towards the target distance R_{12}. If the applied restraint would otherwise act to deviate the atomic distance away from R_{12}, no energy is added. In this work, we use Amsterdam Modeling Suite (AMS2024),[57] and the CHON2017_weak_bb force field developed by Vashisth et al.[51] This force field has been widely used to capture chemical kinetics and thermo-mechanical behavior in epoxies[40,51] and vitrimers.[11]

Force parameter selection by Bayesian optimization

Selecting appropriate values for the restraint energy force parameters (F_1 and F_2 in Equation 2) is essential to ensure realistic and controlled reaction energies. Inappropriate values may

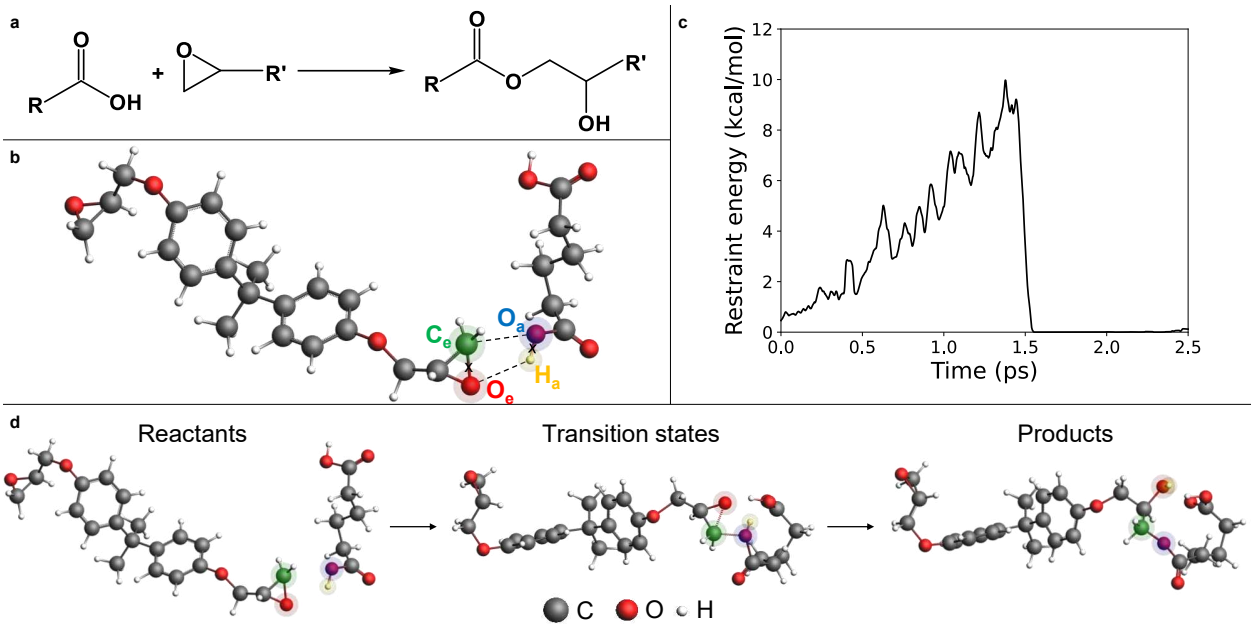

Figure 1: Accelerated ReaxFF for curing reactions. (a) Scheme of the curing reaction between a carboxylic acid and an epoxide. (b) Labeled reactive atoms of three applied restraints. (c) Restraint energy added in each time step during the boost period. The energy values are running-averaged over windows of 200 data points. (d) Reaction coordinates of the curing reaction obtained by Accelerated ReaxFF.

result in side reactions or polymer chain scission, leading to unwanted byproducts. During an Accelerated ReaxFF simulation, we track the amount of restraint energy added at each time step, with the peak energy serving as an approximation of the activation or barrier energy for a given reaction. Unlike restraint energy E_{rest}, the other energy terms in Equation 1 are not explicitly dependent on force parameters (F_1 and F_2) and their changes are attributed to bonded and non-bonded interactions driven by E_{rest}. Therefore, these force parameters are optimized to minimize the peak restraint energy necessary for successful reactions.

In this work, we consider the curing reactions of epoxides with carboxylic acids as well as the transesterification reactions between two β-hydroxy esters (i.e., bond exchange reactions of vitrimers), as shown in Figure 1a and 2a, respectively. For the curing reactions, the epoxide carbon (C_e), epoxide oxygen (O_e), acid oxygen (O_a) and acid hydrogen (H_a) are labeled as reactive atoms (Figure 1b). For the bond exchange reactions, the ester carbon (C_e), ester oxygen (O_e), hydroxyl oxygen (O_h) and hydroxyl hydrogen (H_h) are labeled as reactive atoms

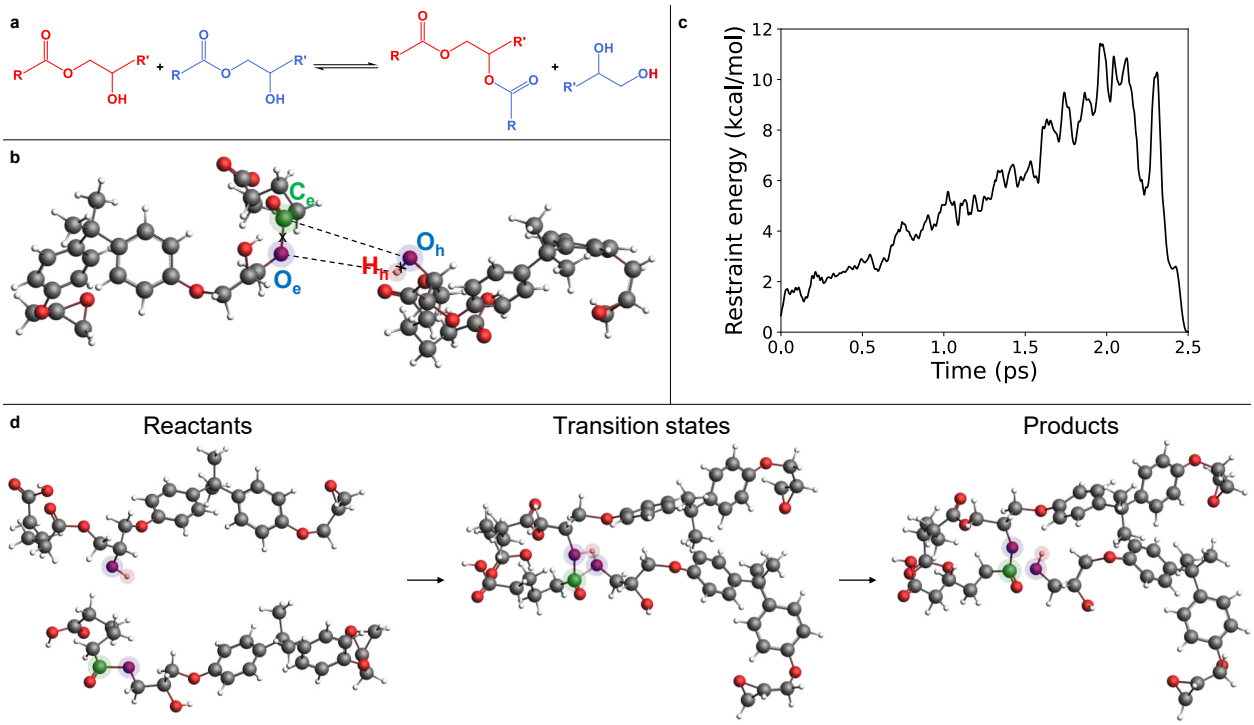

Figure 2: Accelerated ReaxFF for bond exchange reactions. (a) Scheme of the transesterification reaction between two β-hydroxy esters. (b) Labeled reactive atoms of three applied restraints. (c) Restraint energy added in each time step during the boost period. The energy values are running-averaged over windows of 200 data points. (d) Reaction coordinates of the BER obtained by Accelerated ReaxFF.

(Figure 2b), and O_e and O_h are labeled as the same type to make the reaction reversible. For each reaction, we carry out an Accelerated ReaxFF simulation with two monomers and apply three bond boosts to three pairs of reactive atoms for $N = 10,000$ steps. The simulation is performed under NVT ensemble at 423 K (150 °C) for curing and 500 K (227 °C) for BER using Berendsen thermostats with a damping constant of 100 fs. The peak restraint energy is calculated if the reaction is successful, i.e., two old bonds are broken, and two new bonds are formed. To find the 6 force parameters (F_1 and F_2 for three restraints) that give the minimum peak restraint energy, we employ the Bayesian optimization method, which is an iterative algorithm to optimize black-box functions.[58] Other optimization methods, such as grid search or gradient-based optimization, are not feasible due to the high-dimensional and non-differentiable nature, respectively, of our optimization objective. A schematic workflow of Bayesian optimization is presented in Supporting Information (Figure S1). We start with

20 random sets of force parameters as initial guesses and calculate their corresponding peak restraint energy using Accelerated ReaxFF simulation. The data is used to train a surrogate Gaussian process model, which predicts the probabilistic distribution of peak energy as a function of force parameters. The next set of force parameters to probe is predicted by the GP model based on the expected improvement acquisition function, and the corresponding peak energy is calculated and added to the training data for the next iteration. For each reaction, five random initial configurations close to the transition state that satisfy distance ranges are selected, and 100 iterations of Bayesian optimization are performed on each configuration. The force parameters that give the lowest peak restraint energy are adopted for simulations of larger systems to model curing and transesterification reactions.

Preparation of a vitrimer specimen

To cure epoxides with carboxylic acids and create a vitrimer virtual specimen, 150 adipic acid and 150 bisphenol A diglycidyl ether (DGEBA) molecules (1:1 molar ratio) are placed in a cubic simulation box of $70 \times 70 \times 70$ Å^3. Using the optimized force parameters for the curing reaction, we apply restraint energy to the reactive atoms labeled in Figure 1a. The restraint energy is applied to only one group of reactive atoms at the same time (i.e., number of boosts is 1) and lasts for $N = 10,000$ steps of 0.25 fs. The curing simulation is performed under NVT ensemble at 423 K and is terminated when no new bonds between acids and epoxides are formed for 15 ps. Next, the cured system is annealed cyclically between 100 K and 800 K to remove local heterogeneities. More specifically, the cured specimen is first cooled down to 100 K from 423 K (curing temperature) in 25 ps. The subsequent annealing cycles involve heating up to 800 K and cooling down to 100 K with 100 K increments under NPT ensemble. Each cycle takes 155 ps, and the simulation is stopped when the densities of the last two cycles converge.

Temperature-dependent bond exchange reactions

The force parameters for BERs are optimized at 500 K (Figure 2); however, to better simulate temperature-dependent behavior (e.g., non-isothermal creep), we have to make BERs dependent on temperature. To this end, we develop and tune an empirical equation for F_1 force parameter for each pair of reactive atoms:

$$\frac{F_1}{F_1^{500}} = F_0 e^{-\alpha E_a/RT}, \tag{4}$$

where F_1^{500} is the optimized parameter at 500 K, F_0 and α are empirical parameters, $E_a = 14.6$ kcal/mol is the activation energy for transesterification reactions obtained from a previous DFT study,[59] R is the ideal gas constant and T is temperature. At 500 K, $F_1 = F_1^{500}$, which makes α the only tunable parameter. Equation 4, derived from the Arrhenius equation, allows us to capture the probability of chemical reactions at different temperature in ReaxFF simulations.

To verify the effect of temperature-dependent F_1 parameter on probability of reactions, we carry out a series of ReaxFF simulations with different α and temperature. For each simulation, 100 bond boosts are allowed simultaneously to apply restraint energy to reactive atoms, i.e., there are 100 reactions happening in each boost period for $N = 10,000$ steps. Each simulation takes 10 boost periods (25 ps) and the reaction probability is calculated as the ratio of total number of successful BERs to the maximum number of possible reactions (i.e., 1000). For each α value, we check the reaction probability as a function of temperature and select α that gives the most reasonable probability-temperature profile for the non-isothermal creep simulations (discussed later).

Creep simulations of vitrimers

With the annealed virtual specimen and temperature-dependent force parameters, we proceed to carry out non-isothermal creep simulations of vitrimers. Starting with 100 K, we

heat the specimen at a constant rate up to 800 K while applying a constant stress in x direction. The simulation box dimensions in y and z directions are allowed to change under the NPT ensemble. Periodic boundary conditions are applied in all three directions. During the simulations, we monitor the strain in x direction, i.e.,

$$\epsilon_x = l_x(t)/l_x(0) - 1, \tag{5}$$

where $l_x(t)$ and $l_x(0)$ are simulation box dimension at time t and initial dimension at 100 K, respectively. We also track the number of successful BERs occurring throughout the simulations. Simulations are performed with different applied stress levels, heating rates and numbers of boosts to uncover the effect of external stimuli on creep behavior of vitrimers. Due to the large discrepancies in length and time scales between MD simulations and experiments, more significant external stimuli are typically used to accelerate the kinetics in MD simulations.[46,51,60] In this work, the range of applied stress levels are selected to ensure observable creep strain responses. It is also notable that the applied heating rates in ReaxFF simulations are significantly higher than those of experiments to ensure simulations can be completed using the computational resources available. As a result, while some degree of localized chain relaxation is captured, modeling long-range chain relaxation requires coarse-grained simulations which are beyond the scope of this work.[28,31] By controlling the number of boosts, we can regulate the number of simultaneous reactions and effectively simulate the effect of catalyst concentration on reaction rate, and correlate these findings with experiments.

To investigate the structural evolution during creep, we calculate the fractional free volume (FFV) from the MD trajectories at different temperatures. Multiwfn is employed to calculate FFV of vitrimer samples by first dividing the three-dimensional simulation box into small voxels.[61] A voxel is considered free if it is not within the van der Waals radius of any atom and FFV is defined as the number of free voxels divided by the total number of

Table 1: Distance ranges and optimized force parameters (highlighted in bold) for curing reactions.

Atoms	Distance range (Å)	R_{12} (Å)	F_1 (kcal/mol)	F_2 (Å^{-2})
C_e - O_e	1.0 - 1.8	2.50	**70**	**0.25**
C_e - O_a	3.0 - 10.0	1.40	**210**	**0.95**
O_e - H_a	2.5 - 10.0	0.95	**90**	**0.30**
O_a - H_a	0.8 - 1.1	None	None	None

voxels.

The spatial distribution of reactive atoms is essential to reaction dynamics. To this end, we extract the coordinates of all ester carbon atoms from the MD trajectories and quantify their spatial distribution by the normalized average nearest neighbor distance (NND). NND is calculated by

$$\mathrm{NND} = \frac{\frac{1}{n}\sum_{i=1}^{n} d_i}{\left(\frac{V}{n}\right)^{\frac{1}{3}}}, \tag{6}$$

where n is total number of ester carbon atoms, d_i is the distance between atom i and its nearest neighbor, and V is volume of the simulation box. The average nearest neighbor distance is normalized by $\left(\frac{V}{n}\right)^{\frac{1}{3}}$ to remove the effect of box size and number of atoms. A larger NND indicates more dispersed atoms with respective to the simulation box.

Results

Parameters for Accelerated ReaxFF reactions

The optimized parameters that give the smallest restraint energy for curing reactions are listed in Table 1. The total restraint energy of three applied restraints added in each time step is presented in Figure 1c. The peak restraint energy at each Bayesian optimization iteration is shown in Figure S2a (Supporting Information). For each restraint between each pair of reactive atoms, the evolution of the interatomic distance R_{ij}^t, the target distance R_{12}^t

Table 2: Distance ranges and optimized force parameters (highlighted in bold) for bond exchange reactions.

Atoms	Distance range (Å)	R_{12} (Å)	F_1 (kcal/mol)	F_2 (Å^{-2})
C_e - O_e	1.0 - 1.8	2.50	**50**	**0.25**
C_e - O_h	5.0 - 8.0	1.40	**205**	**1.00**
O_e - H_h	5.0 - 8.0	0.95	**250**	**0.25**
O_h - H_h	0.8 - 1.1	None	None	None

and the restraint energy are presented in Supporting Information (Figure S3a). At 1.5 ps, the distance between C_e and O_e rapidly increases to the final target distance $R_{12} = 2.5$ Å, indicating the dissociation of the bond in the epoxide ring. The distance between C_e and O_a decreases to 1.5 Å and the distance between O_e and H_a decreases to 0.95 Å, which demonstrates that new ester bond and hydroxyl bond are formed. The epoxide-carboxylic acid reaction is thereby complete and little restraint energy is added afterwards. Three snapshots of the system showing the reactants, transition states and reaction products are presented in Figure 1d.

For bond exchange reactions (i.e., transesterification reactions between two β-hydroxy esters), the optimized parameters are presented in Table 2. The peak restraint energy as a function of optimization iteration is shown in Figure S2b (Supporting Information). The total restraint energy is plotted in Figure 2c and distance between reactive atoms is presented in Supporting Information (Figure S3b). The bond between C_e and O_e is broken near 2.5 ps and the reaction is complete near the end of the boost period. The peak restraint energy is 15.96 kcal/mol, which is comparable with the activation barrier (14.6 kcal/mol) calculated by Bhusal et al. using DFT.[59] The snapshots in Figure 2d indicate a smooth transition state from reactants to products.

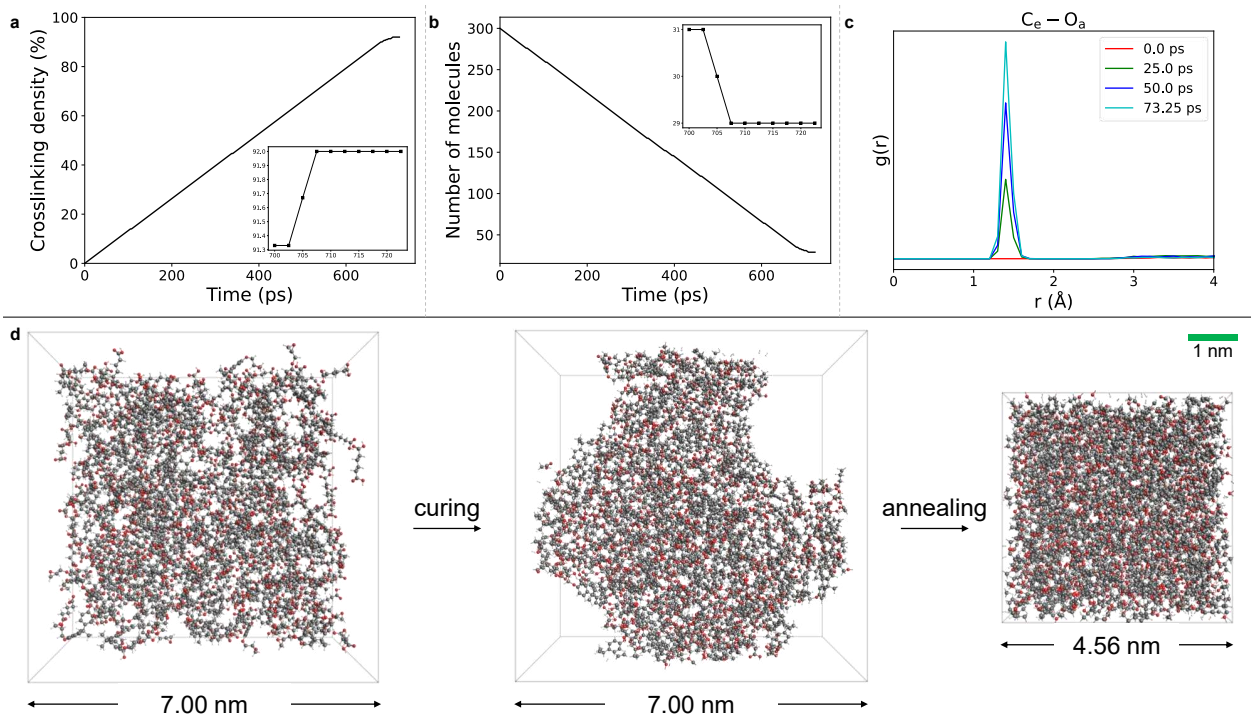

Figure 3: Preparation of the vitrimer virtual specimen. (a) Curing ratio during the Accelerated ReaxFF curing simulation. Inset shows that the curing ratio converges in the end of the simulation. (b) Number of molecules during the simulation simulation time. Inset shows that the number of molecules converges in the end of the simulation. (c) Radial distribution functions between acid oxygen and epoxide carbon atoms during curing simulation. (d) Snapshots of the monomer system, cured system and annealed system. The local heterogeneities are removed by the annealing procedures.

Preparation of vitrimer virtual specimen

With the optimized parameters for Accelerated ReaxFF, we proceed to create a vitrimer virtual specimen. 150 pairs of adipic acid and DGEBA molecules (with 1:1 stoichiometric ratio of epoxides and carboxyl groups) are placed in a simulation box and restraint energy is successively applied to one group of reactive atoms. The curing ratio (defined as the ratio of number of formed ester bonds to the maximum number of theoretical bonds between C_e and O_a) and number of molecules are presented in Figure 3a and 3b as functions of simulation time. Both values converge in the last 15 ps of the simulation, which indicates that no new bond is formed and the system is reacted thoroughly. The cured system has

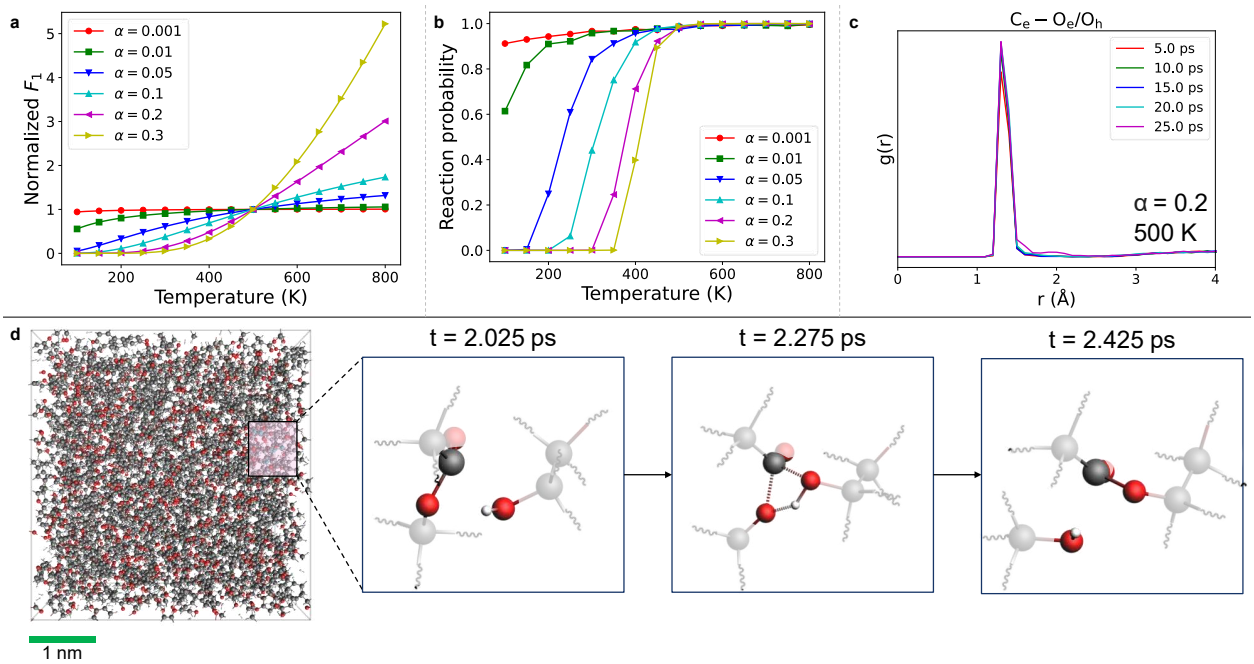

Figure 4: Bond exchange reactions in the vitrimer system at different temperature. (a) Normalized F_1 parameter as a function of α parameter and temperature. (b) Probability of successful BERs as a function of α parameter and temperature. (c) Radial distribution functions between ester carbon and hydroxyl/ester oxygen atoms during the simulation with $\alpha = 0.2$ at 500 K. (d) Snapshots of the vitrimer system highlighting reactive atoms of a successful BER.

a final curing ratio of 92%. The radial distribution functions between acid oxygen and epoxide carbon atoms are presented in Figure 3c and the increasing peak intensity at 1.4 Å indicates the formation of new C_e-O_a bonds during the simulation. Movie S1 (Supporting Information) provides a comprehensive view of the entire curing simulation. To remove the local heterogeneities and prepare a homogeneous specimen for further simulations, we anneal the cured structure in cycles between 100 K and 800 K. The density converges by fifth cycle (Figure S4) and local heterogeneities are greatly reduced (Figure 3d).

Temperature-dependent bond exchange reactions

Next we examine the variation of F_1 as function of temperature and α (see Equation 4), and resulting reaction probabilities in Accelerated ReaxFF simulations. The F_1 parameter normalized by F_1^{500} (optimized F_1 parameters at 500 K as presented in Table 2) based on

different α parameters and temperature according to Equation 4 is presented in Figure 4a. At low α values, F_1 is approximately equal to F_1^{500} and barely changes with temperature. At high α values, $F_1 \sim 0$ at low temperature but rises quickly at higher temperature. The probability of BERs as a function of α and temperature is presented in Figure 4b. Across a broad range of α values, the BER probability varies significantly and a reasonable value is selected for simulations based on the reaction probability as per reported experimental observations.[6,11,62–64] At $\alpha = 0.001$ where F_1 barely changes with temperature, reaction probability is maintained at a high level (larger than 0.9) regardless of temperature and the lowest probability is observed at 100 K due to limited mobility of atoms and polymer chains. At $\alpha \geq 0.05$, the reaction probability shows a gradual transition from 0 to 1 with increasing temperature and the transition range increases with α. Specifically, at $\alpha = 0.2$, the transition happens between 300 K and 500 K, which agrees well with the experimental observations for transesterification vitrimers.[6,11,62–64] Therefore, we select $\alpha = 0.2$ for non-isothermal creep simulations later. Figure 4c presents the radial distribution functions (RDF) between ester carbon and hydroxyl/ester oxygen atoms (hydroxyl oxygen and ester oxygen are treated as the same type for reversible BERs, as described in Methods) with during the simulation with $\alpha = 0.2$ at 500 K. The RDF peak intensity stays constant around 1.4 Å and demonstrates the preserved carbon-oxygen bonds and integrity of the associative covalent adaptive network with the ongoing BERs. Figure 4d shows the relevant atoms of a BER and validates the capability of the Accelerated ReaxFF setup to simulate multiple chemical reactions in a large polymer system.

Creep behavior of vitrimers

We next examine the strain-temperature behavior for non-isothermal creep on virtual vitrimer specimens with varying external stimuli (see also Movie S2-4 in Supporting Information). The top row in Figure 5 shows the evolution of strain during non-isothermal creep of vitrimers and the effect of stress level, heating rate and number of boosts. The insets

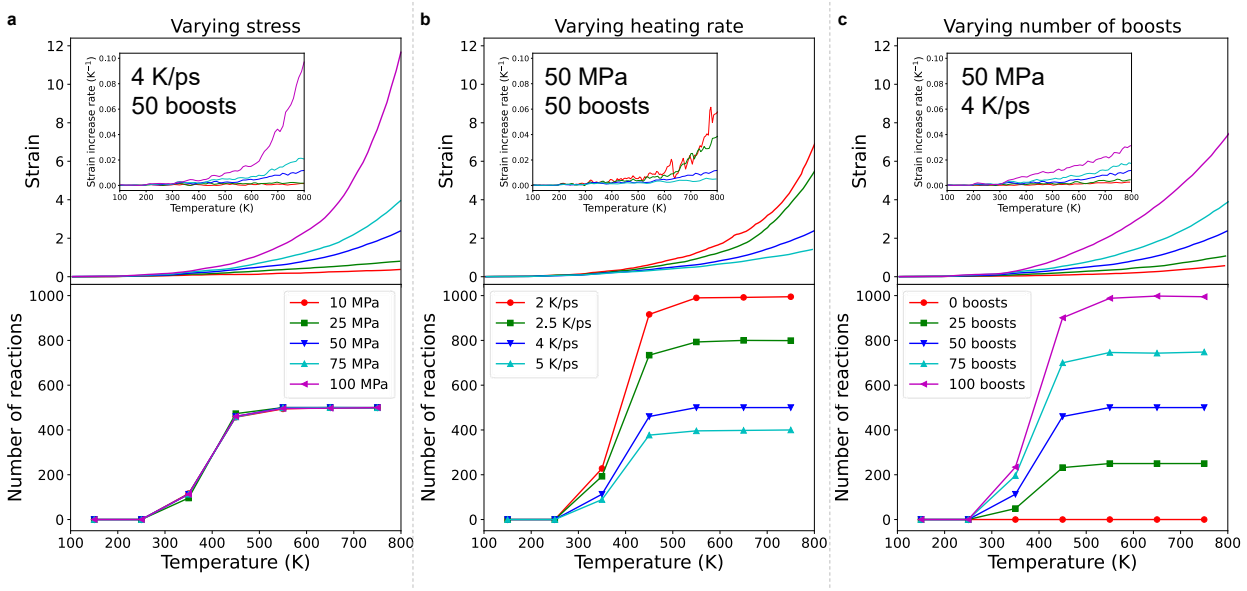

Figure 5: Creep strain (top) and number of reactions (bottom) at different temperature during non-isothermal creep simulations with (a) varying stress, (b) varying heating rate and (c) varying number of boosts. The insets show the creep increase rates with respective to temperature.

present the derivative of strain with respect to temperature, i.e., the strain increase rate. Note that the number of bond boosts controls the maximum number of BERs taking place simultaneously and simulates the effect of catalyst concentration in actual experiments. It is observed that increasing stress leads to larger creep strain accumulated at a higher rate. Lower heating rate and larger number of boosts have a similar effect by increasing BERs (see Figure 5 bottom row), thereby making vitrimers more malleable to external stress. By contrast, higher applied stress has little effect on number of BERs or probability of successful reaction, which is governed by F_1 parameter and Equation 4. In all cases, the strain and number of reactions start to develop after 300 K which is the defined onset temperature of BERs (see Figure 4b). This indicates that the effect of all three external stimuli is driven by BERs simulated using Accelerated ReaxFF. All three trends presented in our ReaxFF simulations agree well with experimental results by Hubbard et al. who observed an increase in creep strain with increasing applied force from 0.5 to 1 N, decreasing heating rate from 10 to 2 °C/min and increasing catalyst concentration from 1 to 3 mol%.[35] Similar observations

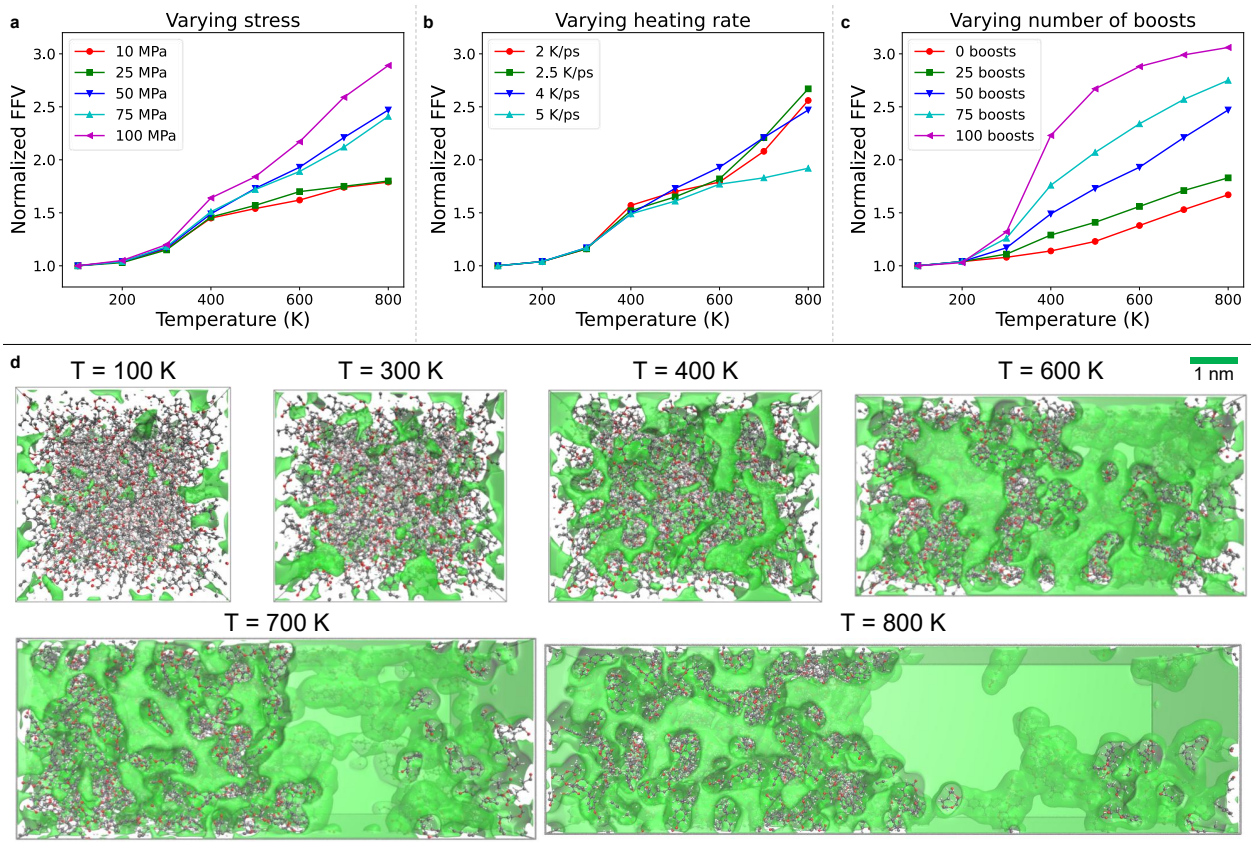

Figure 6: Fractional free volume (FFV) in the vitrimer during non-isothermal creep simulations with (a) varying stress, (b) varying heating rate and (c) varying number of boosts. (d) Snapshots of the simulation box at different temperature from the simulation with 50 MPa applied stress, 4 K/ps heating rate and 50 boosts. The FFV values are normalized by the FFV of initial configuration at 100 K.

were reported by other previous experimental studies.[36,65]

To verify the capabilities of Accelerated ReaxFF in reducing side reactions and unwanted bond dissociation, we calculate the fraction of intended bond dissociation events (i.e., the ratio of number of bond dissociation events between reactive atoms to the total number of bond dissociation events), as presented in Figure S5 (Supporting Information). Most of the bond dissociation events (over 99%) involve reactive atoms in bond exchange reactions, demonstrating the ability of the Accelerated ReaxFF framework to suppress side reactions even at high temperature.

The evolution of fractional free volume (FFV) normalized by the FFV at 100 K is presented in Figure 6. Similar to creep strain results, higher applied stress and more bond

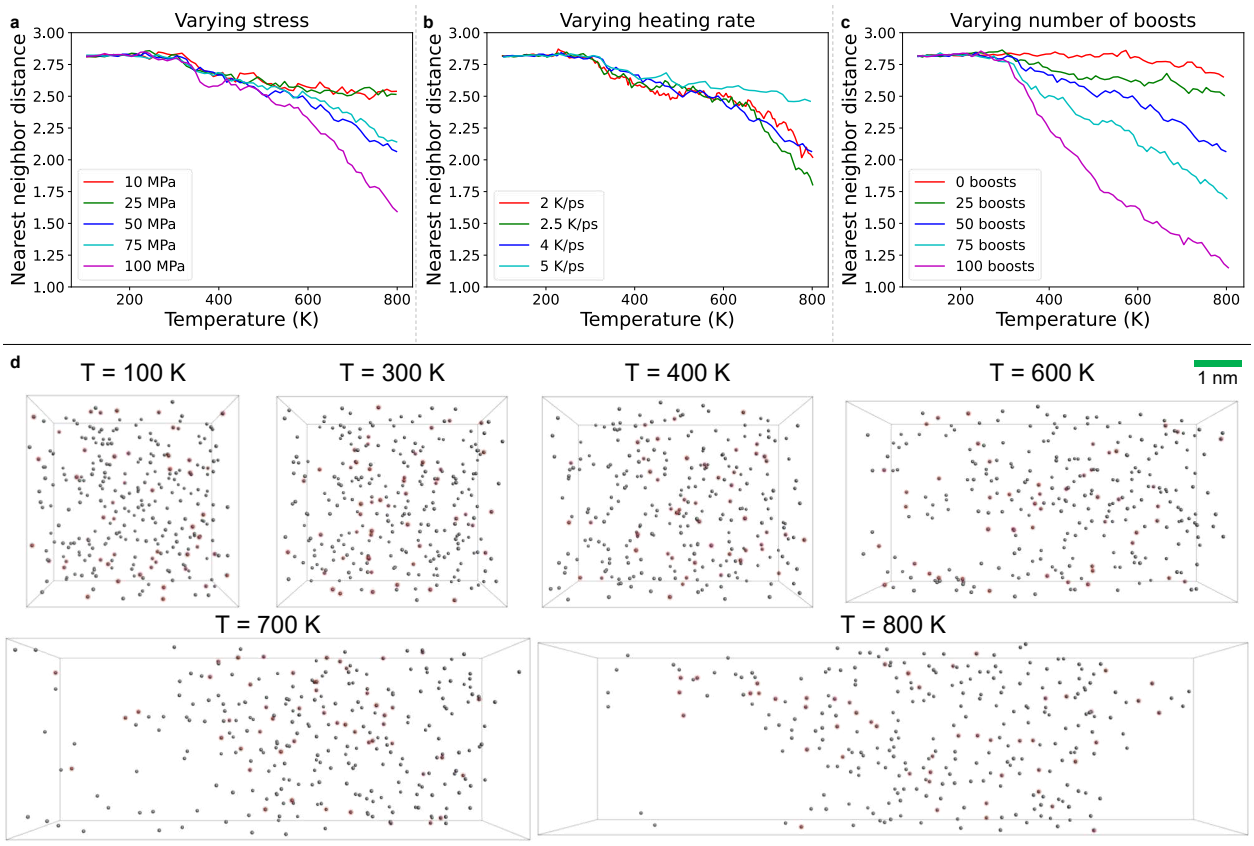

Figure 7: Average normalized nearest neighbor distances of all ester carbon atoms in the vitrimer during non-isothermal creep simulations with (a) varying stress, (b) varying heating rate and (c) varying number of boosts. (d) The spatial distribution of ester carbon atoms at different temperature from the simulation with 50 MPa applied stress, 4 K/ps heating rate and 50 boosts. The ester carbon atoms involved in BERs are highlighted in red.

boosts lead to larger free volume. However, no significant effect of heating rate below 4 K/ps is observed. This can be attributed to the fact that the vitrimer chains under lower heating rates are given more time to adapt themselves, thereby balancing the effect of increasing strain induced by more BERs. Visualizations of free volume for the simulation with 50 MPa applied stress, 4 K/ps heating rate and 50 boosts are presented in Figure 6d. Large pores start to develop around 600 K and lead to final rupture at 800 K.

We select the ester carbon atoms as a representative of the reactive atoms and quantify their spatial distribution by normalized average nearest neighbor distance (NND), which is plotted in Figure 7. NND the is largest for the initial configuration at 100 K, which is attributed to the short-range and long-range interactions between atoms in polymer chains

which prevent the atoms from clustering (Figure 7a-c). As temperature increases, NND in all cases decreases and follows the exact opposite trend to free volume. The correlation between NND and fractional free volume is shown in Supporting Information (Figure S6). When there is free volume in the system, atoms are confined in specific regions in the simulation box while absent in the voids (Figure 7d). Therefore, the atoms are more clustering and lead to a lower NND. The NND of ester carbon atoms that are involved in activated BERs (i.e., the ester carbon atoms which the restraint energy is added to) is presented in Figure S7. The trends are much less significant with large fluctuations since these atoms are changed every boost period for $N = 10,000$ steps.

The distribution of successful BERs between ester carbon and hydroxyl oxygen atoms is presented in Supporting Information (Figure S8). Most atom pairs never satisfy the distance requirements through the whole simulation while five reactions occur between a pair of atoms (see Figure S8a,b in Supporting Information). The positions of that atom pair when the reaction is activated is shown in Figure S8c, presenting the varying relative orientations of the reactive atoms from successful BERs at high temperature. The number of atom pairs involved in 1 to 6 successful BERs during each creep simulations is presented in Figure S9, which appears to decrease with increasing number of reactions. The applied stress has no effect on the atom pair number, whereas decreasing heating rate or increasing number of boosts increases the number of atom pairs by increasing the total number of successful BERs in the simulation.

Conclusion

In this work, we applied the Accelerated ReaxFF framework to simulate curing and bond exchange reactions in vitrimers with associative covalent adaptive network, and investigated non-isothermal creep behavior of vitrimers. Unlike traditional cutoff-based methods in MD which ignore the reaction dynamics, the Accelerated ReaxFF method can capture the reac-

tion pathways during MD simulations by providing an additional restraint energy to reactive atoms. Bayesian optimization was employed to identify the appropriate force parameters by minimizing the peak restraint energy added during the bond boost. The optimized parameters were utilized to carry out curing reactions of carboxylic acids and epoxides to form a vitrimer system with a realistic curing ratio. To capture the temperature-dependent BERs in vitrimers, we introduced an empirical equation for force parameter F_1 with respective to temperature. The developed framework was utilized to model non-isothermal creep behavior of vitrimers. The effect of varying applied stress, heating rate and number of boosts was investigated and the findings align well with experimental results. In addition, this study provides insights on evolution of bond exchange reactions and free volume, spatial distribution of reaction sites and localization of reactions at different temperature during non-isothermal creep. The proposed framework, with Bayesian optimization to select parameters for curing and bond exchange reactions, can be applied to other classes of vitrimers and provide atomistic insights into vitrimer behavior under various conditions.

Supporting Information

Schematic workflow of Bayesian optimization; evolution of peak restraint energy during Bayesian optimization; distance between reactive atoms and corresponding restraint energy during bond boost; density of the system in the last three cycles of annealing simulations; fraction of intended bond dissociation from non-isothermal creep simulations; correlation between normalized fractional free volume and nearest neighbor distance of all ester carbon atoms from non-isothermal creep simulations; nearest neighbor distance of ester carbon atoms involved in bond exchange reactions from non-isothermal creep simulations; distribution of successful BERs between each pair of ester carbon and hydroxyl oxygen atoms; number of atom pairs involved in 1 to 6 successful BERs during non-isothermal creep simulations; movies of the curing and creep simulations.

Acknowledgments

AV would like to acknowledge the support of Air Force Summer Faculty Fellowship, 2024. This work was completed using the advanced computational, storage, and networking infrastructure provided by the Hyak supercomputer system at the University of Washington, Seattle. Funding supporting this work was partially provided by the US National Science Foundation (grant CMMI-2421235).

References

(1) Bilyeu, B.; Brostow, W.; Menard, K. P. Epoxy thermosets and their applications I: chemical structures and applications. *Journal of Materials Education* **1999**, *21*, 281–286.

(2) Guo, Q. *Thermosets: structure, properties, and applications*; Woodhead Publishing, 2017.

(3) Utekar, S.; Suriya, V.; More, N.; Rao, A. Comprehensive study of recycling of thermosetting polymer composites–Driving force, challenges and methods. *Composites Part B: Engineering* **2021**, *207*, 108596.

(4) Morici, E.; Dintcheva, N. T. Recycling of thermoset materials and thermoset-based composites: challenge and opportunity. *Polymers* **2022**, *14*, 4153.

(5) Post, W.; Susa, A.; Blaauw, R.; Molenveld, K.; Knoop, R. J. A review on the potential and limitations of recyclable thermosets for structural applications. *Polymer reviews* **2020**, *60*, 359–388.

(6) Montarnal, D.; Capelot, M.; Tournilhac, F.; Leibler, L. Silica-like malleable materials from permanent organic networks. *Science* **2011**, *334*, 965–968.

(7) Scheutz, G. M.; Lessard, J. J.; Sims, M. B.; Sumerlin, B. S. Adaptable crosslinks in polymeric materials: resolving the intersection of thermoplastics and thermosets. *Journal of the American Chemical Society* **2019**, *141*, 16181–16196.

(8) Chakma, P.; Konkolewicz, D. Dynamic covalent bonds in polymeric materials. *Angewandte Chemie International Edition* **2019**, *58*, 9682–9695.

(9) Shi, Q.; Yu, K.; Kuang, X.; Mu, X.; Dunn, C. K.; Dunn, M. L.; Wang, T.; Qi, H. J. Recyclable 3D printing of vitrimer epoxy. *Materials Horizons* **2017**, *4*, 598–607.

(10) Biswal, A. K.; Nandi, A.; Wang, H.; Vashisth, A. Ultrasonic welding of fiber reinforced vitrimer composites. *Composites Science and Technology* **2023**, *242*, 110202.

(11) Kamble, M.; Vashisth, A.; Yang, H.; Pranompont, S.; Picu, C. R.; Wang, D.; Koratkar, N. Reversing fatigue in carbon-fiber reinforced vitrimer composites. *Carbon* **2022**, *187*, 108–114.

(12) Chen, F.; Cheng, Q.; Gao, F.; Zhong, J.; Shen, L.; Lin, C.; Lin, Y. The effect of latent plasticity on the shape recovery of a shape memory vitrimer. *European polymer journal* **2021**, *147*, 110304.

(13) Li, B.; Zhu, G.; Hao, Y.; Ren, T. Shape reconfiguration and functional self-healing of thermadapt shape memory epoxy vitrimers by exchange reaction of disulfide bonds. *Smart Materials and Structures* **2022**, *31*, 095047.

(14) Zhang, Z.; Biswal, A. K.; Nandi, A.; Frost, K.; Smith, J. A.; Nguyen, B. H.; Patel, S.; Vashisth, A.; Iyer, V. Recyclable vitrimer-based printed circuit boards for sustainable electronics. *Nature Sustainability* **2024**, 1–12.

(15) Li, W.; Xiao, L.; Huang, J.; Wang, Y.; Nie, X.; Chen, J. Bio-based epoxy vitrimer for recyclable and carbon fiber reinforced materials: Synthesis and structure-property relationship. *Composites Science and Technology* **2022**, *227*, 109575.

(16) Ma, Y.; Jiang, X.; Shi, Z.; Berrocal, J. A.; Weder, C. Closed-Loop Recycling of Vinylogous Urethane Vitrimers. *Angewandte Chemie International Edition* **2023**, *62*, e202306188.

(17) McBride, M. K.; Worrell, B. T.; Brown, T.; Cox, L. M.; Sowan, N.; Wang, C.; Podgorski, M.; Martinez, A. M.; Bowman, C. N. Enabling applications of covalent adaptable networks. *Annual review of chemical and biomolecular engineering* **2019**, *10*, 175–198.

(18) Kloxin, C. J.; Bowman, C. N. Covalent adaptable networks: smart, reconfigurable and responsive network systems. *Chemical Society Reviews* **2013**, *42*, 7161–7173.

(19) Yang, Y.; Xu, Y.; Ji, Y.; Wei, Y. Functional epoxy vitrimers and composites. *Progress in Materials Science* **2021**, *120*, 100710.

(20) Biswal, A. K.; Hong, P.; Zhang, Z.; Zheng, Y.; Gupta, S.; Nepal, D.; Iyer, V.; Vashisth, A. Flexible and Stretchable Vitrimers for Sustainable Electronics. *ACS Applied Materials & Interfaces* **2025**,

(21) Li, K.; Tran, N. V.; Pan, Y.; Wang, S.; Jin, Z.; Chen, G.; Li, S.; Zheng, J.; Loh, X. J.; Li, Z. Next-Generation Vitrimers Design through Theoretical Understanding and Computational Simulations. *Advanced Science* **2024**, *11*, 2302816.

(22) Long, R.; Qi, H. J.; Dunn, M. L. Modeling the mechanics of covalently adaptable polymer networks with temperature-dependent bond exchange reactions. *Soft Matter* **2013**, *9*, 4083–4096.

(23) Smallenburg, F.; Leibler, L.; Sciortino, F. Patchy particle model for vitrimers. *Physical review letters* **2013**, *111*, 188002.

(24) Rovigatti, L.; Nava, G.; Bellini, T.; Sciortino, F. Self-dynamics and collective swap-driven dynamics in a particle model for vitrimers. *Macromolecules* **2018**, *51*, 1232–1241.

(25) Ciarella, S.; Sciortino, F.; Ellenbroek, W. G. Dynamics of vitrimers: Defects as a highway to stress relaxation. *Physical review letters* **2018**, *121*, 058003.

(26) Oyarzún, B.; Mognetti, B. M. Efficient sampling of reversible cross-linking polymers: Self-assembly of single-chain polymeric nanoparticles. *The Journal of chemical physics* **2018**, *148*.

(27) Sciortino, F. Three-body potential for simulating bond swaps in molecular dynamics. *The European Physical Journal E* **2017**, *40*, 1–4.

(28) Zhao, H.; Duan, P.; Li, Z.; Chen, Q.; Yue, T.; Zhang, L.; Ganesan, V.; Liu, J. Unveiling the Multiscale Dynamics of Polymer Vitrimers Via Molecular Dynamics Simulations. *Macromolecules* **2023**, *56*, 9336–9349.

(29) Hamzehlou, S.; Ruipérez, F. Computational study of the transamination reaction in vinylogous acyls: Paving the way to design vitrimers with controlled exchange kinetics. *Journal of Polymer Science* **2022**, *60*, 1988–1999.

(30) Guo, X.; Gao, F.; Chen, F.; Zhong, J.; Shen, L.; Lin, C.; Lin, Y. Dynamic enamine-one bond based vitrimer via amino-yne click reaction. *ACS Macro Letters* **2021**, *10*, 1186–1190.

(31) Wu, J.-B.; Li, S.-J.; Liu, H.; Qian, H.-J.; Lu, Z.-Y. Dynamics and reaction kinetics of coarse-grained bulk vitrimers: a molecular dynamics study. *Physical Chemistry Chemical Physics* **2019**, *21*, 13258–13267.

(32) Perego, A.; Khabaz, F. Volumetric and rheological properties of vitrimers: a hybrid molecular dynamics and Monte Carlo simulation study. *Macromolecules* **2020**, *53*, 8406–8416.

(33) Xia, J.; Kalow, J. A.; Olvera de la Cruz, M. Structure, Dynamics, and Rheology of Vitrimers. *Macromolecules* **2023**, *56*, 8080–8093.

(34) Li, L.; Chen, X.; Jin, K.; Torkelson, J. M. Vitrimers designed both to strongly suppress creep and to recover original cross-link density after reprocessing: quantitative theory and experiments. *Macromolecules* **2018**, *51*, 5537–5546.

(35) Hubbard, A. M.; Ren, Y.; Konkolewicz, D.; Sarvestani, A.; Picu, C. R.; Kedziora, G. S.; Roy, A.; Varshney, V.; Nepal, D. Vitrimer transition temperature identification: coupling various thermomechanical methodologies. *ACS Applied Polymer Materials* **2021**, *3*, 1756–1766.

(36) Hubbard, A. M.; Ren, Y.; Picu, C. R.; Sarvestani, A.; Konkolewicz, D.; Roy, A. K.; Varshney, V.; Nepal, D. Creep mechanics of epoxy vitrimer materials. *ACS Applied Polymer Materials* **2022**, *4*, 4254–4263.

(37) Leimkuhler, B.; Matthews, C. Molecular dynamics. *Interdisciplinary applied mathematics* **2015**, *39*.

(38) Hospital, A.; Goñi, J. R.; Orozco, M.; Gelpí, J. L. Molecular dynamics simulations: advances and applications. *Advances and Applications in Bioinformatics and Chemistry* **2015**, 37–47.

(39) Varshney, V.; Patnaik, S. S.; Roy, A. K.; Farmer, B. L. A molecular dynamics study of epoxy-based networks: cross-linking procedure and prediction of molecular and material properties. *Macromolecules* **2008**, *41*, 6837–6842.

(40) Vashisth, A.; Ashraf, C.; Bakis, C. E.; van Duin, A. C. Effect of chemical structure on thermo-mechanical properties of epoxy polymers: Comparison of accelerated ReaxFF simulations and experiments. *Polymer* **2018**, *158*, 354–363.

(41) Odegard, G. M.; Patil, S. U.; Deshpande, P. P.; Kanhaiya, K.; Winetrout, J. J.; Heinz, H.; Shah, S. P.; Maiaru, M. Molecular dynamics modeling of epoxy resins using the reactive interface force field. *Macromolecules* **2021**, *54*, 9815–9824.

(42) Odegard, G. M.; Patil, S. U.; Gaikwad, P. S.; Deshpande, P.; Krieg, A. S.; Shah, S. P.; Reyes, A.; Dickens, T.; King, J. A.; Maiaru, M. Accurate predictions of thermoset resin glass transition temperatures from all-atom molecular dynamics simulation. *Soft Matter* **2022**, *18*, 7550–7558.

(43) Li, C.; Strachan, A. Molecular simulations of crosslinking process of thermosetting polymers. *Polymer* **2010**, *51*, 6058–6070.

(44) Odegard, G. M.; Jensen, B. D.; Gowtham, S.; Wu, J.; He, J.; Zhang, Z. Predicting mechanical response of crosslinked epoxy using ReaxFF. *Chemical Physics Letters* **2014**, *591*, 175–178.

(45) Yang, H.; Yu, K.; Mu, X.; Shi, X.; Wei, Y.; Guo, Y.; Qi, H. J. A molecular dynamics study of bond exchange reactions in covalent adaptable networks. *Soft Matter* **2015**, *11*, 6305–6317.

(46) Singh, G.; Varshaney, V.; Sundararaghavan, V. Understanding creep in vitrimers: Insights from molecular dynamics simulations. *Polymer* **2024**, 127667.

(47) Islam, M. S.; Lee, J.; Varshney, V.; Nepal, D.; Roy, A. K. Self-healing and thermal transport behavior in catalytic vitrimer-graphene composite. *Composites Science and Technology* **2024**, *257*, 110835.

(48) Senftle, T. P.; Hong, S.; Islam, M. M.; Kylasa, S. B.; Zheng, Y.; Shin, Y. K.; Junkermeier, C.; Engel-Herbert, R.; Janik, M. J.; Aktulga, H. M.; others The ReaxFF reactive force-field: development, applications and future directions. *npj Computational Materials* **2016**, *2*, 1–14.

(49) Karuth, A.; Alesadi, A.; Vashisth, A.; Xia, W.; Rasulev, B. Reactive molecular dynamics study of hygrothermal degradation of crosslinked epoxy polymers. *ACS Applied Polymer Materials* **2022**, *4*, 4411–4423.

(50) Bhati, M.; Senftle, T. P. Identifying adhesion properties at Si/polymer interfaces with ReaxFF. *The Journal of Physical Chemistry C* **2019**, *123*, 27036–27047.

(51) Vashisth, A.; Ashraf, C.; Zhang, W.; Bakis, C. E.; Van Duin, A. C. Accelerated ReaxFF simulations for describing the reactive cross-linking of polymers. *The Journal of Physical Chemistry A* **2018**, *122*, 6633–6642.

(52) Dasgupta, N.; Yilmaz, D. E.; Van Duin, A. Simulations of the biodegradation of citrate-based polymers for artificial scaffolds using accelerated reactive molecular dynamics. *The Journal of Physical Chemistry B* **2020**, *124*, 5311–5322.

(53) Vermeersch, L.; Wang, T.; Van den Brande, N.; De Vleeschouwer, F.; van Duin, A. Computational Insights into Tunable Reversible Network Materials: Accelerated ReaxFF Kinetics of Furan-Maleimide Diels–Alder Reactions for Self-Healing and Recyclability. *The Journal of Physical Chemistry A* **2024**,

(54) Van Duin, A. C.; Dasgupta, S.; Lorant, F.; Goddard, W. A. ReaxFF: a reactive force field for hydrocarbons. *The Journal of Physical Chemistry A* **2001**, *105*, 9396–9409.

(55) Mortier, W. J.; Ghosh, S. K.; Shankar, S. Electronegativity-equalization method for the calculation of atomic charges in molecules. *Journal of the American Chemical Society* **1986**, *108*, 4315–4320.

(56) Miron, R. A.; Fichthorn, K. A. Accelerated molecular dynamics with the bond-boost method. *The Journal of chemical physics* **2003**, *119*, 6210–6216.

(57) Te Velde, G. t.; Bickelhaupt, F. M.; Baerends, E. J.; Fonseca Guerra, C.; van Gisbergen, S. J.; Snijders, J. G.; Ziegler, T. Chemistry with ADF. *Journal of Computational Chemistry* **2001**, *22*, 931–967.

(58) Shahriari, B.; Swersky, K.; Wang, Z.; Adams, R. P.; De Freitas, N. Taking the human

out of the loop: A review of Bayesian optimization. *Proceedings of the IEEE* **2015**, *104*, 148–175.

(59) Bhusal, S.; Oh, C.; Kang, Y.; Varshney, V.; Ren, Y.; Nepal, D.; Roy, A.; Kedziora, G. Transesterification in vitrimer polymers using bifunctional catalysts: modeled with solution-phase experimental rates and theoretical analysis of efficiency and mechanisms. *The Journal of Physical Chemistry B* **2021**, *125*, 2411–2424.

(60) Rigby, D.; Roe, R.-J. Molecular dynamics simulation of polymer liquid and glass. I. Glass transition. *The Journal of chemical physics* **1987**, *87*, 7285–7292.

(61) Lu, T.; Chen, F. Multiwfn: A multifunctional wavefunction analyzer. *Journal of computational chemistry* **2012**, *33*, 580–592.

(62) Zhang, B.; Li, H.; Yuan, C.; Dunn, M. L.; Qi, H. J.; Yu, K.; Shi, Q.; Ge, Q. Influences of processing conditions on mechanical properties of recycled epoxy-anhydride vitrimers. *Journal of Applied Polymer Science* **2020**, *137*, 49246.

(63) Chen, J.-H.; Liu, B.-W.; Lu, J.-H.; Lu, P.; Tang, Y.-L.; Chen, L.; Wang, Y.-Z. Catalyst-free dynamic transesterification towards a high-performance and fire-safe epoxy vitrimer and its carbon fiber composite. *Green Chemistry* **2022**, *24*, 6980–6988.

(64) Zheng, Y.; Thakolkaran, P.; Biswal, A. K.; Smith, J. A.; Lu, Z.; Zheng, S.; Nguyen, B. H.; Kumar, S.; Vashisth, A. AI-Guided Inverse Design and Discovery of Recyclable Vitrimeric Polymers. *Advanced Science* **2024**, 2411385.

(65) Kaiser, S.; Novak, P.; Giebler, M.; Gschwandl, M.; Novak, P.; Pilz, G.; Morak, M.; Schlögl, S. The crucial role of external force in the estimation of the topology freezing transition temperature of vitrimers by elongational creep measurements. *Polymer* **2020**, *204*, 122804.

TOC Graphic

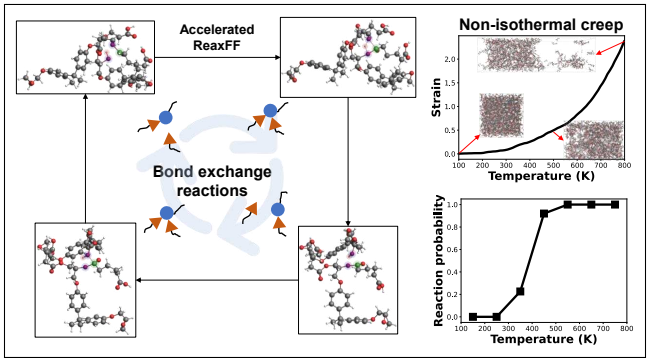
Accelerated
ReaxFF
Bond exchange
reactions
Non-isothermal creep
Strain
Temperature (K)
Reaction probability
Temperature (K)